High-pressure melting behavior of tin up to 105 GPa

R. Briggs,[1,*] D. Daisenberger,[2] O. T. Lord,[3] A. Salamat,[4] E. Bailey,[5] M. J. Walter,[3] and P. F. McMillan[1,†]

[1]*Department of Chemistry, University College London, 20 Gordon Street, Kings Cross, London WC1H 0AJ, United Kingdom*

[2]*Diamond Light Source Ltd., Diamond House, Harwell Science Campus, Didcot, Oxfordshire OX11 0DE, United Kingdom*

[3]*School of Earth Sciences, University of Bristol, Wills Memorial Building, Queen's Road, Bristol BS8 1RJ, United Kingdom*

[4]*Department of Physics and Astronomy and HiPSEC, University of Nevada, Las Vegas, Nevada 89154, USA*

[5]*Department of Earth Sciences, University College London, Gower Street, London WC1E 6BT, United Kingdom*

(Received 18 June 2016; revised manuscript received 19 December 2016; published 3 February 2017)

The melting curve of Sn initially rises steeply as a function of pressure but exhibits a decrease in slope (dT_m/dP) above 40 GPa to become nearly flat above 50 GPa. Previous studies have argued that a body-centered tetragonal (bct) to cubic (bcc) phase transition occurs in this range at room temperature. However, our investigations have shown that the phase behavior is more complex in this region with orthorhombic (bco) splitting of reflections occurring in the x-ray diffraction pattern above 32 GPa and coexisting diffraction signatures of bco and bcc structures are observed between 40 and 70 GPa. Here we have documented the simultaneous presence of bco and bcc reflections up to the melting point, negating the possibility that their coexistence might indicate a kinetically hindered first-order phase transformation. In this paper we have extended the observation of Sn melting relations into the megabar ($P > 100$ GPa) range using the appearance of liquid diffuse scattering in x-ray diffraction patterns and discontinuities during thermal signal processing to diagnose the occurrence of melting. Both techniques yield consistent results that indicate the melting line maintains the same low slope up to the highest pressure examined and does not flatten. The results below approximately 40 GPa agree well with the melting relations produced recently using a multiphase equation of state fitted to available or assumed data. Above this pressure the experimental melting points lie increasingly below the predicted crystal-liquid phase boundary, but above the flat melting from past studies, indicating that the thermodynamic properties of the body-centered "γ"-Sn structure remain to be clarified.

DOI: 10.1103/PhysRevB.95.054102

I. INTRODUCTION

Tin occupies an intermediate position between semiconducting (Si, Ge) and metallic (Pb) members of the group 14 elements and it therefore exhibits unusual bonding changes and structural polymorphism as a function of pressure and temperature. A metallic β-Sn phase with its atoms in distorted octahedral coordination is stable at ambient conditions but upon cooling below 13.5 °C slowly transforms into the diamond-structured α-Sn allotrope [1]. The transition is accompanied by a 27% volume expansion, resulting in the phenomenon known as "tin disease." The phase relations under combined high P-T conditions are relatively well understood below 20 GPa [2]. During compression at room temperature, β-Sn transforms into a body-centered γ-Sn polymorph above 10.8 GPa, initially exhibiting a tetragonal distortion (bct) from cubic symmetry [3–5]. The initial value of the axial distortion is approximately $c/a \sim 0.91$. The melting temperature rises steadily and steeply as a function of pressure above the β-Sn–bct–liquid triple point (Fig. 1).

Recent experiments at room temperature reveal that the γ-Sn polymorph evolves into an orthorhombic (bco) structure at 32.5 GPa before it becomes fully cubic (bcc) with $c/a = 1$ above 70 GPa [5]. There is an unusual coexistence between the characteristic x-ray reflections of bco and bcc structures that is maintained at room temperature between 40–70 GPa. Previous studies have suggested that this might correspond to a kinetically impeded first-order phase transition between bct and bcc polymorphs. However, our recent work involving careful analysis of the x-ray diffraction patterns combined with DFT calculations indicated that the observed coexistence of the x-ray signatures results from the simultaneous presence of nano- to mesoscale domains of orthorhombic and cubic types of axially strained domains within a single γ-Sn phase [5]. This unusual situation arises because of the lack of any barrier against c/a or b/a lattice distortions relative to the zero-point vibrational energy of a perfect infinite crystal. The bcc γ-Sn form remains stable at ambient temperature until 157 GPa above which a hexagonal close-packed (hcp) polymorph is observed to appear [6,7]. First-principles theoretical predictions using *ab initio* random structure searching (AIRSS) techniques indicate that a bcc polymorph then becomes reentrant above 1300 GPa (1.3 TPa) as a novel electride phase containing discrete clumps of electron density localized between the atomic cores [6].

The melting temperature (T_m) of Sn at ambient pressure is 505 K and the negative Clapeyron slope of the β-γ transformation results in a triple point occurring at 583 K and 3.3 GPa (Fig. 1) [2,8]. Beyond this triple point dT_m/dP exhibits a slight increase as required by the thermodynamic constraints for the free energy relations between pairs of coexisting polymorphs approaching a three-phase invariant point. At higher pressures the melting of the γ-Sn phase was first examined using dynamic shock loading techniques. Analysis of data along the principal Hugoniot indicates that incipient melting begins at 50 GPa and 2300 K [9]. In the same work, discontinuities in particle velocity observed upon

*Present address: European Synchrotron Radiation Facility, BP-220, F-38043 Grenoble Cedex, France.

†p.f.mcmillan@ucl.ac.uk

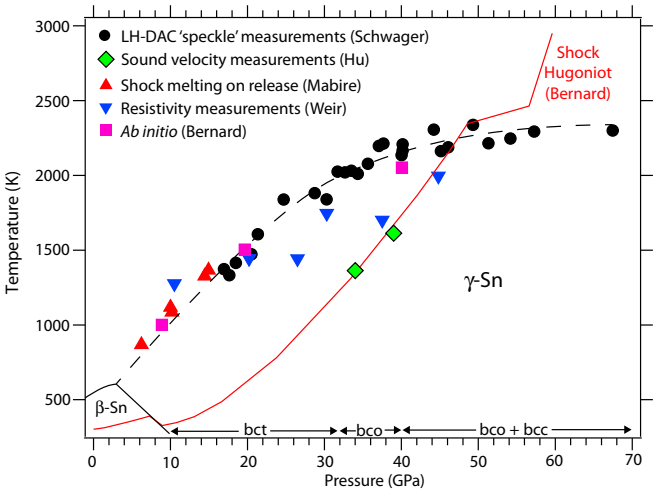

FIG. 1. Current understanding of the phase diagram of Sn. Room temperature compression experiments reveal structural transformations from tetragonal (bct) to orthorhombic (bco) to cubic body-centered (bcc) structures [5]. The slope of the melting line decreases beyond 30 GPa to become nearly flat, $dT_m/dP \sim 0$, above 38 GPa (circles) [11]. This corresponds to the pressure range at which apparent coexistence of bco and bcc structures is observed in x-ray diffraction patterns at low temperature [5].

release from shocked states allowed the melting relation to be traced down to 6 GPa (Fig. 1) [9]. The experimental data agreed with the results of *ab initio* molecular dynamics simulations that indicated a melting slope that slightly decreased at higher pressures [10]. The melting curve of Sn was also studied using static diamond anvil cell techniques (DAC) combined with laser heating. These data, which used the onset of motion in the "speckle" pattern created by a visible laser reflected from the sample surface as the melting criterion, agreed well with the previous shock loading and theoretical results [11]. Together, these studies indicate a melting line with markedly decreasing dT_m/dP above 40 GPa such that it reaches only ~2200 K by 68 GPa (Fig. 1). Resistively heated diamond anvil cell data, with *in situ* resistance measurements, have also suggested a rise in the melting slope up to 40 GPa, though there is a large spread in the data, especially in the 25–40 GPa range, falling mainly below the other data [12]. In a first study to examine this problem we used laser-heating (LH) DAC techniques combined with synchrotron x-ray scattering to study the onset of melting at pressures into the megabar range ($P > 100$ GPa) [13]. However, in that previous experiment no detailed discussion was given to the unexpected results, which led to the new experiments we report here.

Because these melting data are typically incorporated in databases used to predict and analyze the behavior of Sn-based materials over a wide range of P-T conditions it is important to extend our knowledge of the melting behavior to higher pressure values. Our preliminary analysis of the LH-DAC + x-ray diffraction data indicated a dramatic increase in T_m occurring above 70 GPa, reaching 5500 ± 500 K by 105 GPa [13]. However, that result raised questions concerning the thermodynamics of the crystalline phase and its melting properties in the high-P regime that we found difficult to understand. In the present study we have reexamined the melting relations in the same high P-T range using LH-DAC melting experiments with the onset of melting determined by the first appearance of liquid scattering [$S(Q)$] in the synchrotron x-ray diffraction patterns. We have also carried out additional melting studies between 74–105 GPa using discontinuities during thermal signal processing to diagnose melting [14,15]. Our new results indicate that the melting line continues with a shallow dT_m/dP slope, rising slightly above the previous melting curve.

II. EXPERIMENTAL METHODS

A. *In situ* x-ray diffraction

Diamond anvils with 300, 200, and 150/300 μm (beveled) culets were used for LH-DAC experiments carried out at the European Synchrotron Radiation Facility (ESRF) using Re as the gasket material. Sn powder (99.99% Aldrich, packed under Ar) was pressed into a thin foil < 10 μm thick and loaded into the gasket hole surrounded by NaCl or KBr (to provide a pressure-transmitting medium, or PTM) that also acted as thermal insulation between the sample and the diamonds. LH-DAC experiments were carried out at beamline ID27 of the ESRF, with an x-ray wavelength of 0.3738 Å, using a diode-pumped 40W Nd^{3+}:YAG laser ($\lambda = 1064$ nm) or a 100W Yb^{3+} doped fiber laser ($\lambda = 1070.4$ nm) focused on the sample from both sides [16,17]. The laser spot was slightly defocused to create a heating area of ~20 μm diameter. Laser-heating experiments and the determination of melting criteria from x-ray diffraction measurements are further discussed in Refs. [17–20]. Initial pressures were determined from the room temperature equation of state of NaCl before later being refined using the room temperature equation of state of Sn [5]. Sample pressures were recorded before and after laser heating and a thermal pressure correction was applied using $P_{TH} = \alpha K_T (T_m - T_{300})$ for NaCl. For KBr loadings, the thermal pressure was corrected using an experimentally determined empirical formula as described in Lord *et al.* [15].

Once heating was established the laser power was increased steadily, with thermal emission and x-ray data collected continuously during the T ramp. Thermal emission data were collected from a 2×2 μm^2 area. Diffracted x rays were collected from the same area with an x-ray spot size of $\sim3\times2$ μm^2. The alignment of the x-ray beam with the laser-heated spot was checked before and after each heating run by ensuring that the fluorescence of the x-ray beam was co-located with the pinhole used to collect the thermal emission from the sample for temperature measurement. X-ray patterns were obtained with 1 s exposures every few seconds resulting in several hundred patterns accumulated during each melting run. The first appearance of liquid scattering [$S(Q)$] in the diffraction pattern was taken to indicate the onset of melting (Fig. 2). Temperatures were determined by analyzing thermal emission data collected between 400–950 nm using reflective objectives using both Planck and Wien fits. Temperatures determined in this way are expected to be reliable to within $\pm$100 K for temperatures up to 4000 K [16].

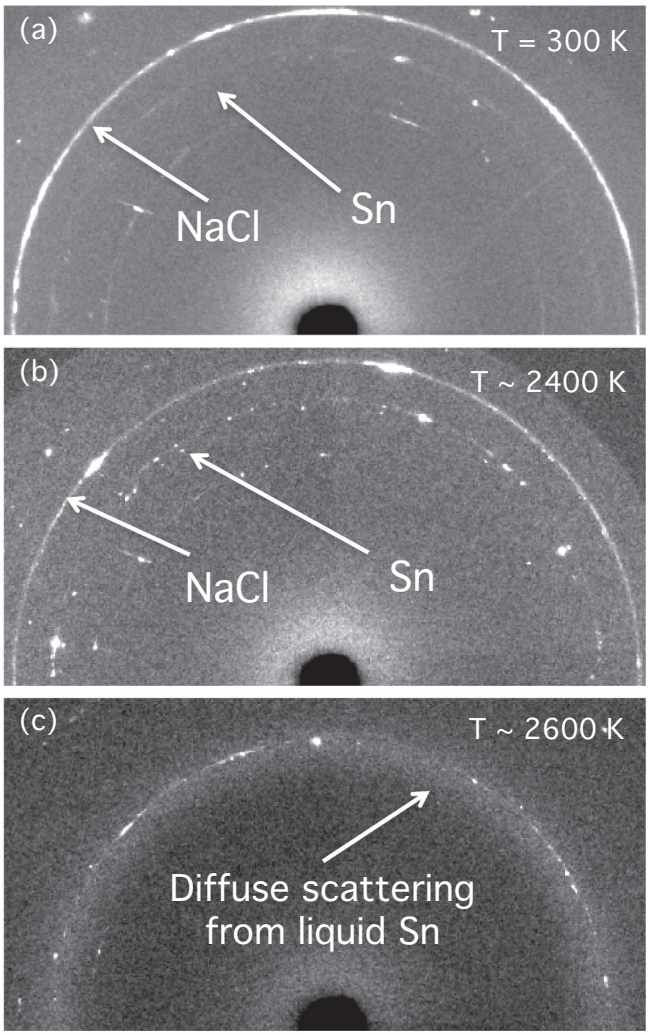

FIG. 2. Sequence of diffraction images taken during a temperature ramp from a typical LH-DAC ESRF run at an initial pressure of 46 GPa and then heated, revealing the onset of melting at $T \sim 2600$ K as the first appearance of a diffuse scattering ring in the data, superimposed on the diffraction spots from crystalline regions remaining within the sample. The contrast of data at $T \sim 2600$ K was adjusted to emphasize the diffuse scattering "halo."

B. Thermal signal processing

A further series of LH-DAC experiments were carried out at the School of Earth Sciences, University of Bristol. The experimental loading procedure was similar to that described above, except that the sample consisted of high-purity Sn wire (99.99% Aldrich) and MgO was used as the PTM and thermal insulation [14]. One experiment was also performed using KBr as the PTM to provide a comparison with the ESRF experiments. Pressure was monitored during compression before and after laser heating using the fluorescence of submicron Cr:Al_2O_3 (ruby) grains dispersed within the sample chamber, with thermal pressure corrections to the final pressures. Further details of typical sample assemblies along with the laser heating and temperature measurement system are described in Lord *et al.* [14]. Samples were heated using an on-axis double-sided geometry using two 100W diode pumped TEM_{00} Yb^3 doped fiber lasers ($\lambda = 1070$ nm). The power to the lasers was automatically increased in a linear fashion as a function of time, with a constant offset designed to equalize the initial temperature at the two sample surfaces. Temperature cross sections were determined using spectroradiometry from both sides of the sample, whereas imaging radiometry was used to measure 2-D temperature maps on the left-hand side only [15]. The onset of melting was established from the appearance of plateaus or other related distinctive features in the relationship between the incident laser power and temperature recorded in the experiments (see Fig. 3). This melting criterion has been applied in many previous investigations to determine melting in a wide variety of substances [20–22] and it has been directly correlated with the appearance of liquid $S(Q)$ during *in situ* x-ray diffraction experiments in the LH-DAC [14,20].

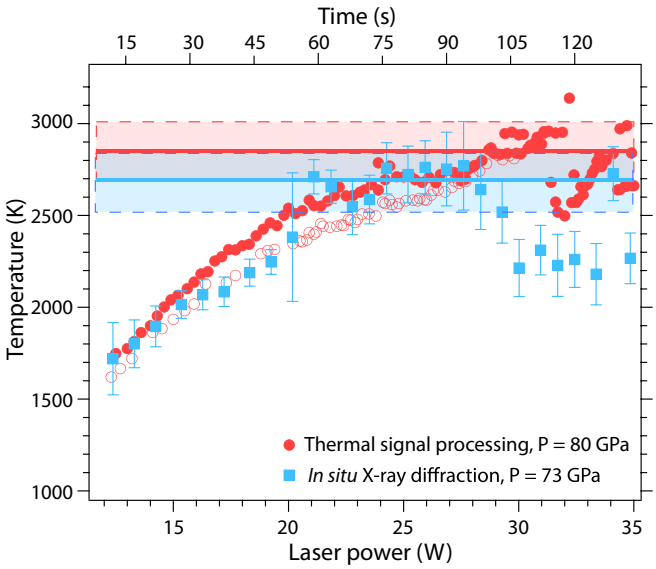

FIG. 3. Typical results from two LH-DAC experiments on Sn as the incident laser power increased linearly as a function of time. The red circles represent apertured spectroradiometry measurements from an off-line experiment at Bristol (closed symbols from the right-hand side of the sample, open symbols from the left-hand side). The blue squares show temperature data from an *in situ* x-ray diffraction experiment, at similar pressure, at ESRF for comparison (top axis). The red and blue bars represent the estimate of the melting temperature and its standard deviation.

III. RESULTS AND DISCUSSION

At pressures below 72 GPa melting points were determined using the onset of liquid diffuse scattering observed in the x-ray experiments as a diagnostic of the melting event. Our data agree very well with those obtained previously using the "speckle" method (Fig. 4), and indicate a steady rise in melting temperature to achieve $T \sim 2400 \pm 100$ K at $P \sim 52$ GPa [11]. Above this value, both our *in situ* x-ray measurements and laser power-temperature measurements indicate a decrease in the dT_m/dP slope such that T_m increases by only 500 K between 50 and 105 GPa (Fig. 4).

One possible explanation for the rapid decrease in melting slope above $P \sim 30$–40 GPa is that the liquid might undergo an

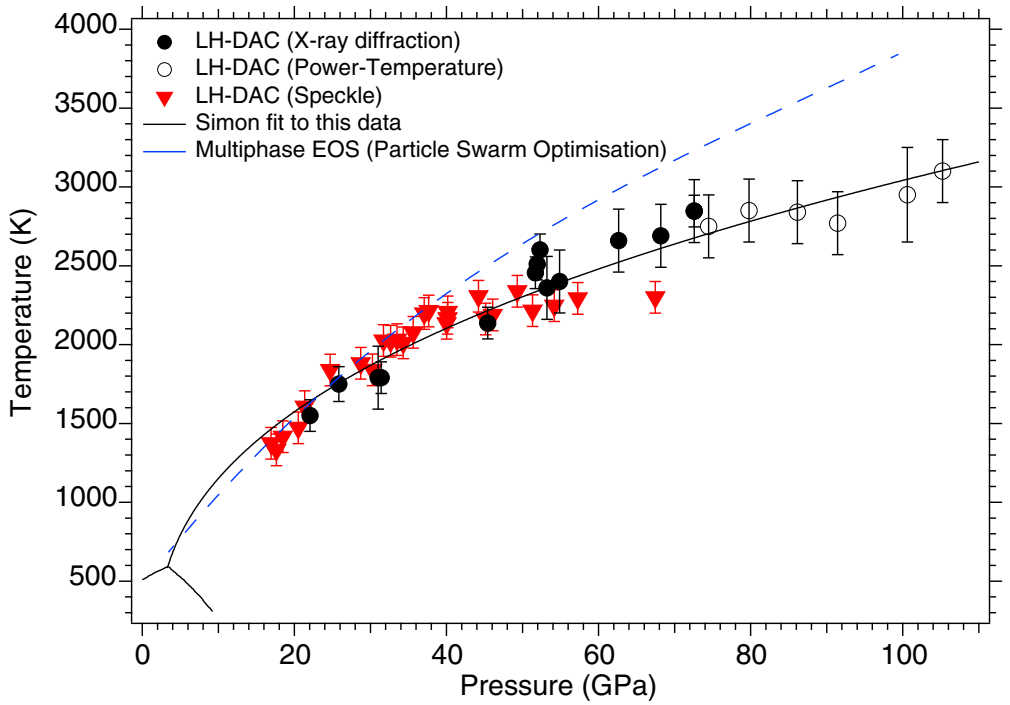

FIG. 4. Melting curve of Sn to $P \sim 100$ GPa. LH-DAC "speckle" data are shown in red triangles [11]. A Simon fit to this data (combination of x-ray diffraction and power-temperature techniques) is depicted as the solid black line. The solid red line represents the recent multiphase equation of state model optimized using particle swarm optimization techniques [23].

unusual structural transformation or densification mechanism in this pressure range. However, synchrotron x-ray scattering studies of liquid Sn up to $P \sim 20$ GPa show no indication of any impending structural change and MD simulation studies at higher P do not suggest any evidence for a polyamorphic transition [24]. Another explanation for the rapid decrease in the melting slope is to consider an unusual decrease in stability of the crystalline phase within the 30–40 GPa range.

We have already presented evidence for such crystalline instability of the γ-Sn phase beginning in this pressure range from room temperature x-ray diffraction experiments combined with DFT calculations [5]. At 10.8 GPa, following room temperature compression, the body-centered phase initially exhibits a tetragonal (bct: $c/a = 0.95$–0.97) distortion that evolves into an orthorhombic (bco) structure above 32.5 GPa. The x-ray reflections are then joined by a second set of peaks indicating the simultaneous presence of a body-centered cubic (bcc) structure above 40 GPa (Fig. 5). The bco and bcc diffraction signatures continue to coexist up to 70 GPa beyond which only bcc diffraction lines are detected [5].

It was initially proposed that the observed coexistence of diffraction patterns could indicate a kinetically hindered first-order phase transition [7,25]. However, our *in situ* x-ray data obtained using LH-DAC techniques show that the coexistence of the bco and bcc diffraction patterns are maintained all the way up to the melting point (Fig. 5). In addition, the same set of coexisting diffraction signatures reappears upon cooling from the liquid state. This behavior would not be consistent with a kinetically hindered bco-bcc transition existing within the system. It might be argued that the apparent coexistence of bco and bcc reflections could be associated with large temperature gradients present within the sample during the LH-DAC experiments [26]. However, the fact that the coexistence is maintained over a temperature range of ~2000 K argues against that possibility and would not explain the observation of coexistence at 300 K. Our proposal is that the bco and bcc diffraction peaks arise from nanoscale domains that express different c/a and b/a axial ratios that are developed spontaneously within the γ-Sn crystallites, due to the absence of an energetic barrier against such distortion throughout the 40–70 GPa range indicated by first-principles calculations for the perfect crystalline model [5]. At high T, the "coexistence" phenomenon persists because the equilibrium must still be maintained.

In some descriptions of the Sn phase diagram the γ-Sn polymorph is identified with the bct/bco structure whereas the bcc structure is taken to represent a second phase. In fact, a γ-bcc-liquid triple point was one of the boundary conditions used to establish the multiphase equation of state (EOS), with particle swarm optimization (PSO), of Cox and Christie [23]. However, our analysis indicates that no such crystalline transition exists within the system, and we retain the designation "γ-Sn" to describe the body-centered phase with all values of the axial distortion parameter. In support of our argument we observe that the dT_m/dP melting slope maintains a constant downward curvature throughout the 40 GPa region, that would not be consistent with the presence of a γ-bcc-liquid triple point where the melting slope would increase.

Previous high-pressure melting studies in the LH-DAC have found that the results can be complicated by reactions occurring between the samples and pressure-transmitting medium. In the case of Ta melting, the formation of TaC was documented in one series of experiments until the diamond

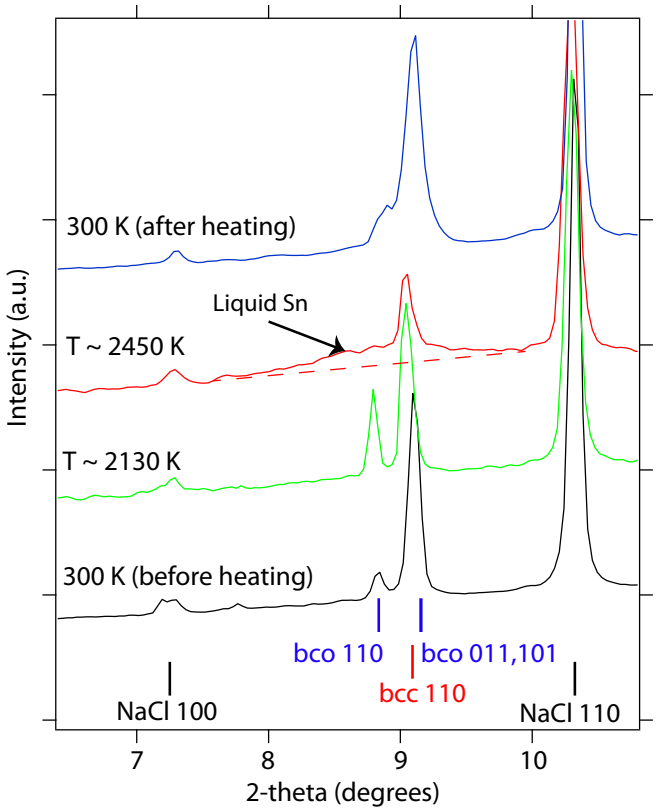

FIG. 5. X-ray diffraction data for γ-Sn in the region of the bco 011, 101, and 110 reflections and the bcc 110 reflection. Diffraction data shown were obtained at an initial pressure of 46 GPa during laser heating experiments showing the persistence of the coexisting bco and bcc reflections up to at least 2130 K, just below the melting temperature. The small shift of the peaks to larger d spacing with increasing temperature occurs due to thermal expansion. After quenching from the liquid to room temperature, the bco and bcc reflections both remain present. There is a small broadening of the peaks (increase of ~0.03 degrees in peak width of bcc 110 and bco 011, 101 peaks) in the quenched diffraction profile. The quenched sample is at slightly higher pressure and as a consequence the bco peaks are closer together and the bcc peak is more pronounced at the expense of the bco 011, 101 peak intensities. These results are in accordance with the results presented in the room temperature compression study of Salamat *et al.* [5]. The weak peaks near 7.7 degrees and apparent splitting of the NaCl 100 peak are due to single spots (independent from sample or insulation diffraction peaks) that are present in 2D diffraction images. These experimental artifacts are less pronounced in the laser-heated images due to the shorter exposure times and do not change position.

anvil surfaces were coated with an oxide layer designed to prevent C diffusion towards the metallic sample [27]. In studies of Pb melting, combined with *in situ* x-ray diffraction, reactions between the sample and the NaCl PTM were evident when temperatures exceeded 4000 K [25]. While no *ex situ* chemical analysis could be carried out in this study, one advantage of using the *in situ* x-ray diffraction technique to diagnose melting is that it can simultaneously determine the presence or absence of some reaction products during the high pressure–high temperature experiments. In the present study of Sn melting we found no evidence for carbide formation or any other reaction. The absence of any SnC formation is interesting as SiC polymorphs form well-known ceramic phases, and GeC can be produced as nanomaterials in vapor deposition experiments. Although no binary Pb or Sn carbides have ever been reported, ternary compounds containing these elements have been produced that represent important semiconducting materials [28].

In our previous preliminary study, we reported evidence for an abrupt steepening in the melting slope at $P \sim 70$ GPa that might have indicated a triple point occurring at this higher pressure [13]. However, we have now carefully reexamined those data in this study, and complemented the x-ray scattering determinations of melting with thermal signal processing in the 75–105 GPa range. Up to ~ 56 GPa, our data are in good agreement with those of Schwager *et al.*, beyond which the two studies diverge by up to 400 K at 68 GPa (the upper pressure limit of the Schwager data). This difference is beyond the mutual uncertainties of the measurements. Extrapolating the fit to the Schwager data to 105 GPa (the upper pressure limit of our data) the discrepancy reaches ~600 K. The slope of the melting curve immediately after the β-Sn–bct–liquid triple point ($P \sim 3$–10 GPa) reveals a $dT_m/dP \sim 88$ K/GPa, a higher melting slope than any other metal [29]. Between 10 and 40 GPa, the melting slope lowers to $dT_m/dP \sim 32$ K/GPa, similar to the LH-DAC + "speckle" data of Schwager *et al.* [11]. Above 50 GPa, our results indicate that the value for dT_m/dP becomes more shallow with $dT_m/dP \sim 15$ K/GPa.

Here we reexamine the $P > 70$ GPa data sets in detail. In these experiments KBr was used to thermally insulate the diamond anvils, since the melting temperatures of Sn in this pressure range were beginning to approach the melting curve of NaCl [30]. The temperature-time profiles from those experiments reveal two distinct temperature plateaus, an example of which is shown as the blue points in Fig. 6. With reference to the experiments performed at similar pressures using MgO as the pressure medium as well as in the *in situ* XRD experiments at lower pressures, the first of the two plateaus (after the start of the temperature ramp) clearly represents the melting of Sn. Therefore, the second plateau likely represents the melting of the KBr PTM. An analogous result was obtained when KBr was used as the PTM in an off-line experiment (the red points in Fig. 6). The two melting points for KBr are plotted in Fig. 7 with a new Simon fit including the lower pressure melting data for KBr from Boehler *et al.* [31]. It is therefore likely that the diffuse scattering originally observed in the high-pressure data above 70 GPa came from the KBr PTM rather than the Sn sample, given the close proximity of the d spacings of the main reflections of both materials at those conditions. One possible explanation as to why $S(Q)$ was not observed from the Sn sample at the first plateau is that liquid Sn may have a low viscosity allowing it to continuously diffuse away from the hot spot where it is created and recrystallize in the cooler surrounding regions that are not probed by the x-ray beam [32].

Due to our concerns with interpreting the melting data obtained in the synchrotron x-ray studies above 70 GPa, we reinvestigated the melting temperature between 60 and 100 GPa using the appearance of plateaus as a function of laser power as a diagnostic of the melting event [14]. Such data have been calibrated against x-ray diffraction results in previous

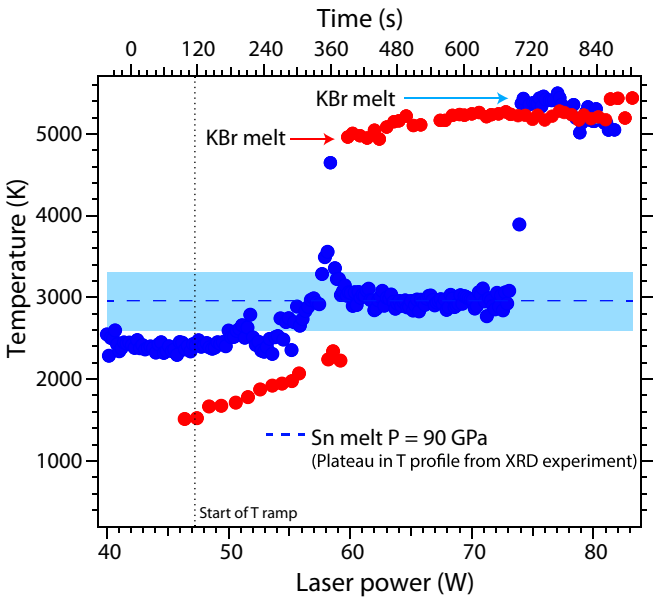

FIG. 6. Comparison of temperature profiles in two separate Sn melting experiments using KBr as insulating material. Power-temperature profiles (red points and bottom axis) for an experiment at $P = 72$ GPa revealing an inflexion at lower temperature (∼2200 K) followed by a plateau at high temperature. An initial plateau in the temperature-time profile is observed also during x-ray diffraction experiments (blue points and top axis), with no liquid scattering observed. A second plateau in the diffraction data set is observed to coincide with an increase in diffuse scattering near the KBr and γ-Sn dominant peaks.

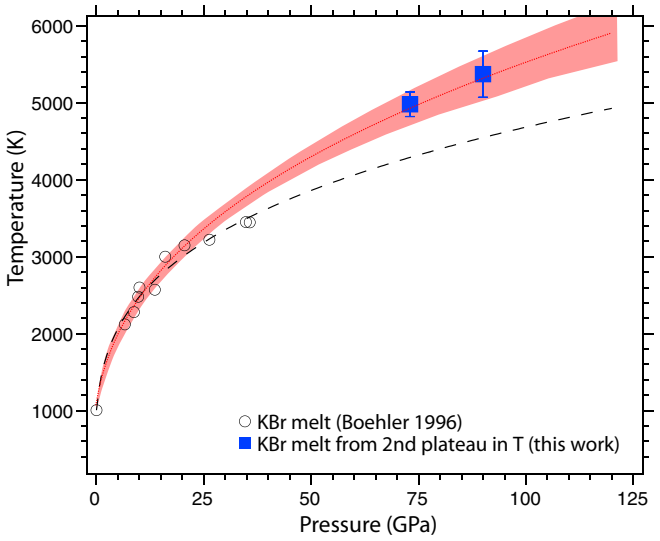

FIG. 7. Melting curve of KBr with Simon fit (open circles and dash line) [31] and melting data of Sn from this experiment (closed circles). The blue squares represent the implied melting points of KBr obtained during these experiments after observing a secondary plateau in laser power-temperature profiles. A new Simon fit to the KBr melting curve is shown in the solid line with bounded area representing the standard error in the fit.

melting studies [14]. The melting points determined in this way continue the increasing trend with a shallow dT_m/dP slope extrapolated from the lower pressure data. A similar T_m relation was found between 40–60 GPa using the "speckle" method although our new data points have slightly greater dT_m/dP slope. Our conclusion is that the melting line of bcc Sn forms a continuous curve with no evidence for any break in slope throughout the range between $P \sim 20$–100 GPa. We have fitted the full set of melting points for the body-centered phase of Sn with a Simon equation, taking the β-γ-liquid triple point as a starting point. The parameters for the new Simon fit to the tin melt curve, valid only for the γ-Sn phase, are given below:

$$T_m = 583\left(\frac{(P_m - 3.3)}{1.4} + 1\right)^{0.39}. \quad (1)$$

Our Simon fit is compared with the melting line established from the recent multiphase EOS with PSO (Fig. 4). The multiphase EOS line passes through the slightly lower T_m values obtained using the "speckle" method in the 20–40 GPa region, crosses our Simon fit at $P \sim 40$ GPa, and then diverges from the experimental data sets with a larger dT_m/dP slope above that value. By 100 GPa, the melting point is overestimated by $\Delta T \sim 500$ K. We suggest that the reason for the discrepancy lies in the assumption that a first-order phase transition is present in the system between γ- and bcc Sn that are considered to be separate "polymorphs", with a resulting γ-bcc-liquid triple point at $P \sim 40$ GPa that was taken as a bounding condition for the multiphase optimization.

In shock compression studies, abrupt changes in sound velocity were determined at 7, 34, and 39 GPa that were assigned to the β-Sn–bct, bct–bcc, and melting transitions, respectively [33]. The incipient melting point identified at 39 GPa (and $T \sim 1550$ K) was significantly lower than the shock melting event observed by Mabire *et al.* ($P \sim 50$ GPa and $T \sim 2300$ K) [9]. We suggest that the sound velocity discontinuities at 34 and 39 GPa could be reinterpreted as due to elastic property changes associated with distortion to the bco structure at $P \sim 34$ GPa followed by appearance of coexisting nanoscale bco + bcc domains within the γ-Sn phase at the higher pressure. Between ∼39 and ∼54 GPa, there is a slight softening of the sound velocity before a significant drop in the calculated shear modulus and yield strength near $P \sim 54$ GPa, that is likely due to melting as indicated by Mabire *et al.* [9].

Recent laser-driven dynamic compression experiments combined with *in situ* x-ray diffraction measurements revealed crystalline Sn existing at up to 1.2 TPa [34]. The *P*-*T* path could not be determined in those experiments, although it must have been bounded by the room temperature isentrope and a second-shock Hugoniot from an initial shock condition at ∼70 GPa [34]. At 1.2 TPa this represents a final-state temperature lying between ∼2000 and ∼10 000 K. Multiple-shock experiments suggest the temperature falls approximately halfway between the isentrope and Hugoniot values [35]. If the same considerations held for the dynamic compression experiments on Sn, the temperature reached at 1.2 TPa would be ∼6000 K. Extrapolation of our Simon fit for bcc melting to that pressure would lead to values of $T_m \sim 11\,000$ K. That would be consistent with the absence of liquid indicated by the diffraction experiments of Lazicki *et al.* [34]. However,

it is likely that a crystalline phase transition occurs in the intervening pressure range between 100 GPa and 1.2 TPa. Several authors have predicted theoretically and Salamat *et al.* have observed experimentally a bcc-hcp transition occurring at 156 GPa. That transition was not observed in the dynamic compression study by Lazicki *et al.* but it could have been obscured by kinetic effects. A second interpretation is that the hcp phase might be limited at high temperature by entropic effects. If the bcc-hcp phase transition does occur within the system and it extends to the melting point, it would likely result in a triple point followed by a further increase in melting temperatures at higher pressure.

IV. CONCLUSION

In this work we have used two complementary laser-heated diamond anvil cell techniques to study and diagnose melting of Sn at pressures into the megabar range. The data show that the melting temperature continues to increase with a shallow slope above 40 GPa. This marked change in melting slope is not consistent with any crystalline phase transition occurring in the 40–70 GPa range but instead reflects a decreased thermodynamic stability of the γ-Sn phase as it encounters a fundamental electronic instability and seeks a nanoscopic domain structure to achieve a thermodynamic ground state [5]. Subsequent experiments carried out at Bristol using thermal signal processing revealed lower melting temperatures than our earlier melting data above 70 GPa [13]; these results are consistent with the extrapolated line from the 40–60 GPa range. The power-temperature data revealed an unusual "sawtooth" pattern that could be explained by the low-viscosity liquid Sn diffusing rapidly away from the laser-heated spot during the DAC experiment [32]. It was then recognized that the liquid $S(Q)$ signals observed in the earlier melting data analysis correspond to melting of the KBr material used as a pressure-transmitting and thermal insulator. That identification provides new constraints on the melting curve of KBr in the 70–90 GPa pressure range.

ACKNOWLEDGMENTS

The authors wish to acknowledge the ESRF for provision of synchrotron radiation facilities on beamline ID27 and the beamline staff for technical assistance during the experiments. The main part of this work was supported by a subcontract to UCL and PFM from the Institute of Shock Physics (ISP) based at Imperial College London, funded by the UK Atomic Weapons Establishment (AWE). R.B. was supported through a Ph.D. studentship awarded through the ISP. The experiments at Bristol were supported by the Natural Environment Research Council through a fellowship awarded to O.T.L. (NE/J018945/1) and a grant awarded to M.J.W. (NE/I010947/1).

[1] S. Gialanella, F. Deflorian, F. Girardi, I. Lonardelli, and S. Rossi, J. Alloys Compd. **474**, 134 (2009).
[2] J. D. Barnett, R. B. Bennion, and H. T. Hall, Science **141**, 1041 (1963).
[3] L.-g. Liu and W. A. Bassett, *Elements, Oxides, and Silicates: High-Pressure Phases with Implications for the Earth's Interior* (Oxford University Press, Oxford, 1986).
[4] S. Desgreniers, Y. K. Vohra, and A. L. Ruoff, Phys. Rev. B **39**, 10359 (1989).
[5] A. Salamat, R. Briggs, P. Bouvier, S. Petitgirard, A. Dewaele, M. E. Cutler, F. Corà, D. Daisenberger, G. Garbarino, and P. F. McMillan, Phys. Rev. B **88**, 104104 (2013).
[6] A. Salamat, G. Garbarino, A. Dewaele, P. Bouvier, S. Petitgirard, C. J. Pickard, P. F. McMillan, and M. Mezouar, Phys. Rev. B **84**, 140104 (2011).
[7] Y. Yao and D. D. Klug, Solid State Commun. **151**, 1873 (2011).
[8] J. D. Dudley and H. T. Hall, Phys. Rev. **118**, 1211 (1960).
[9] C. Mabire and P. L. Hereil, AIP Conf. Proc. **505**, 93 (2000).
[10] S. Bernard and J. B. Maillet, Phys. Rev. B **66**, 012103 (2002).
[11] B. Schwager, M. Ross, S. Japel, and R. Boehler, J. Chem. Phys. **133**, 084501 (2010).
[12] S. T. Weir, M. J. Lipp, S. Falabella, G. Samudrala, and Y. K. Vohra, J. Appl. Phys. **111**, 123529 (2012).
[13] R. Briggs, D. Daisenberger, A. Salamat, G. Garbarino, M. Mezouar, M. Wilson, and P. F. McMillan, J. Phys.: Conf. Ser. **377**, 012035 (2012).
[14] O. T. Lord, I. G. Wood, D. P. Dobson, and L. Vočadlo, Earth Planet. Sci. Lett. **408**, 226 (2014).
[15] O. T. Lord, E. Wann, S. A. Hunt, and A. M. Walker, Phys. Earth Planet. Inter. **233**, 13 (2014).
[16] S. Petitgirard, A. Salamat, P. Beck, and G. Weck, J. Synchrotron Radiat. **21**, 89 (2014).
[17] A. Salamat, R. A. Fischer, R. Briggs, M. I. McMahon, and S. Petitgirard, Coord. Chem. Rev. **277-278**, 15 (2014).
[18] G. Shen, M. L. Rivers, Y. Wang, and S. R. Sutton, Rev. Sci. Instrum. **72**, 1273 (2001).
[19] D. Errandonea, J. Phys. Chem. Solids **67**, 2017 (2006).
[20] D. Santamaría-Pérez, M. Ross, D. Errandonea, G. D. Mukherjee, M. Mezouar, and R. Boehler, J. Chem. Phys. **130**, 124509 (2009).
[21] A. Zerr and R. Boehler, Nature (London) **371**, 506 (1994).
[22] G. Shen, H.-k. Mao, R. J. Hemley, T. S. Duffy, and M. L. Rivers, Geophys. Res. Lett. **25**, 373 (1998).
[23] G. A. Cox and M. A. Christie, J. Phys.: Condens. Matter **27**, 405201 (2015).
[24] T. Narushima, T. Hattori, T. Kinoshita, A. Hinzmann, and K. Tsuji, Phys. Rev. B **76**, 104204 (2007).
[25] A. Dewaele, M. Mezouar, N. Guignot, and P. Loubeyre, Phys. Rev. B **76**, 144106 (2007).
[26] V. Stutzmann, A. Dewaele, J. Bouchet, F. Bottin, and M. Mezouar, Phys. Rev. B **92**, 224110 (2015).
[27] A. Dewaele, M. Mezouar, N. Guignot, and P. Loubeyre, Phys. Rev. Lett. **104**, 255701 (2010).

[28] M. Souadkia, B. Bennecer, and F. Kalarasse, J. Phys. Chem. Solids **74**, 1615 (2013).
[29] D. Errandonea, J. Appl. Phys. **108**, 033517 (2010).
[30] R. Boehler, M. Ross, and D. B. Boercker, Phys. Rev. Lett. **78**, 4589 (1997).
[31] R. Boehler, M. Ross, and D. B. Boercker, Phys. Rev. B **53**, 556 (1996).
[32] See Supplemental Material at http://link.aps.org/supplemental/10.1103/PhysRevB.95.054102 for detailed description and analysis of power vs temperature data. Two 6-panel videos accompany the Supplemental Material, to visualise the temperature changes as a function of time for two melting series. Also included is a table of the melting points determined in this work.
[33] J. Hu, X. Zhou, C. Dai, H. Tan, and J. Li, J. Appl. Phys. **104**, 083520 (2008).
[34] A. Lazicki, J. R. Rygg, F. Coppari, R. Smith, D. Fratanduono, R. G. Kraus, G. W. Collins, R. Briggs, D. G. Braun, D. C. Swift, and J. H. Eggert, Phys. Rev. Lett. **115**, 075502 (2015).
[35] Y. Ping, F. Coppari, D. G. Hicks, B. Yaakobi, D. E. Fratanduono, S. Hamel, J. H. Eggert, J. R. Rygg, R. F. Smith, D. C. Swift, D. G. Braun, T. R. Boehly, and G. W. Collins, Phys. Rev. Lett. **111**, 065501 (2013).